

# Optimal Latency Compensator for Improved Performance of Teleoperated UGVs on Soft Terrains

Ahmad Abubakar , Yahya Zweiri , Ruqayya Alhammadi , Mohammed Mohiudin , Lakmal Seneviratne 

**Abstract**—Bilateral teleoperation of low-speed Unmanned Ground Vehicles (UGVs) on soft terrains is crucial for applications such as space exploration. However, latency arising from transmission delays within the teleoperation system can hinder UGV maneuvering and performance. This paper investigates the impact of latency on the bilateral teleoperation of low-speed UGVs operating on soft terrains and proposes an optimal latency compensator to mitigate this impact for Lunar exploration. Specifically, we propose a genetic algorithm-based predictor framework to optimize the regularization parameters of a model-free predictor. This approach aims to enhance prediction accuracy, thereby improving the performance of the UGV in the presence of latency. Our study revealed a latency threshold of 0.72 seconds is critical for maintaining a stable UGV operation. Furthermore, the proposed predictor framework demonstrates the ability to compensate for the latency by at least 86% Mean Delay Compensation Percentage (MDCP), in contrast to the existing predictor which achieved around 51% for larger delay in the closed-loop teleoperated system. Finally, the developed predictor framework was experimentally validated to compensate for the delays in the teleoperated UGV designed for lunar exploration. The obtained results prove the proposed predictor is effective in compensating for the delays within a closed-loop teleoperated UGV. This effectiveness is showcased through improved performance and transparency.

**Index Terms**—Bilateral Teleoperation, Low-Speed Teleoperated UGV, Latency, Model-free Predictor, Genetic Algorithm

## I. INTRODUCTION

Low-speed teleoperated Unmanned Ground Vehicles (UGVs) have gained significant attention in various fields, including Agricultural operations, military operations, and space exploration tasks [1]. These UGVs are designed to be remotely controlled by human operators, enabling them to perform complex tasks in challenging environments [2]. The concept of teleoperation involves the transfer of control commands from the operator to the UGV and the transmission of sensory information back to the operator [3]. This bidirectional communication, sometimes known as “Bilateral teleoperation”, allows operators to have real-time situational awareness and precise control over the UGV’s

movements and actions [4]. Low-speed teleoperated UGVs are typically used in scenarios that require careful navigation in the remote environment.

Soft terrains present unique challenges for UGV navigation, which can significantly impact the UGV’s maneuverability due to the wheel-terrain interaction, leading to “slippage”. This phenomenon is particularly prevalent in terrains that are unpredictable, such as Regolith. Thus, in order to achieve precise control of the low-speed teleoperated UGV, it is crucial for the operator to be aware of the slippage and apply corrections [5], [6]. By being aware of the slippage, the operator can take proactive measures to adjust the control inputs and ensure overall performance. Haptic feedback could be a good approach to render slippage awareness [6].

One of the key challenges in the bilateral teleoperation system is the presence of latency in the communication channel between the operator and the UGV [3]. This latency can result from various factors, including the communication medium, network bandwidth and congestion, and system architecture [8]. Latency in the bilateral teleoperation system can have a significant impact on the operator’s situational awareness [9], which can result in poor performance and transparency, ultimately leading to instability [4]. Furthermore, the threshold for the latency that causes instability in a system varies depending on the specific system dynamics and application as mentioned in [9], a threshold of 300 milliseconds is a general context [3]. To address the challenges posed by latency in low-speed teleoperated UGVs, researchers have focused on various approaches that include predictive schemes, control techniques, and passivity techniques [10].

### A. Related Work

A bilateral teleoperator system offers a valuable means of communication between human operators and UGVs [4]. Luz et al. [11] highlight the importance of slippage awareness in low-speed teleoperated UGVs through bilateral teleoperators in low-light environments. Obtained results demonstrate that slippage awareness improved task success rates and reduced completion times. In [12], [13], it is demonstrated that haptic feedback can render wheel slippage effectively, thus improving the operator’s understanding of UGV traction. Authors in [5] also render the haptic feedback based on induced wheel velocity loss and propose a compensator scheme to stabilize the system. Similarly, in [14], wheel contact torque was adopted as haptic feedback for traction awareness. Li et al.

This research publication was funded by the KUCARS under Award No. RC1-2018-KUCARS to support the UAE Rashid Rover II project.

A. Abubakar, Y. Zweiri, R. Alhammadi, M. Mohiuddin, and L. Seneviratne are with the Khalifa University Center for Autonomous and Robotic Systems (KUCARS). Y. Zweiri is also associated with the Advanced Research and Innovation Center (ARIC) and the Department of Aerospace Engineering, Khalifa University. L. Seneviratne is also with the Department of Mechanical Engineering at Khalifa University, Abu Dhabi, United Arab Emirates (Corresponding author’s email: 100059792@ku.ac.ae).

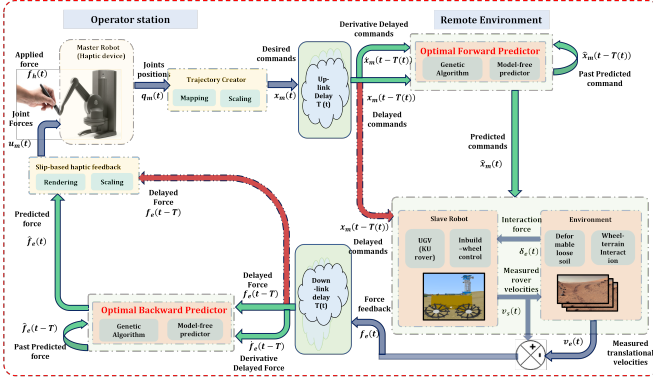


Figure 1: Proposed end-to-end teleoperation of UGV with and without GA-optimized predictor framework. The Red lines represent the Delayed case, and the Green Lines represent the Predicted case.

[15] tackled instability due to processing delays by utilizing the Time Domain Passivity Approach (TDPA) technique and demonstrating improved performance for teleoperated UGVs on soft terrains. However, the aforementioned studies have neglected the consideration of Latency (communication delays), which possess significant practical implications in real-world applications.

Several studies have focused on compensating for communication delays in bilateral teleoperator systems, using various approaches, including the Passivity Approach with the Wave Variable (WV) and TDPA [3], [4]. Other compensation techniques include model-based controls, model-mediated approaches, and model-free approaches [16]. Among these, model-free compensators have been widely employed in teleoperated UGV systems to address the issues of delays, due to the complexities of modeling human driver behavior and the complex nonlinear dynamics of vehicle-environment interactions [9]. The model-free predictor framework proposed by Yingshi Zheng et al. [8] initially introduced a single regularization parameter for compensating delays in general closed network systems. This framework exhibits promising prediction performance that compensates for small delays. Nevertheless, encountered difficulty in handling larger delays and complex empirical data. In a recent study [16], the predictor was modified by introducing additional tuning parameters as a potential solution to compensate for the delays in bilateral teleoperator systems with higher frequency coupling variables, demonstrating improved stability for larger delays. Evaluations conducted on high-speed teleoperated UGVs [17], [18] indicated that this modified predictor yielded more accurate predictions compared to other approaches for UGV bilateral teleoperators. Nonetheless, a major limitation of this predictor is its sensitivity to the turning parameter values, such that even slight deviations from the optimal values can lead to diminished prediction accuracy.

## B. Contributions

The contributions of this work are summarized as follows:

- 1) We investigate the effects of latency on bilateral teleoperation of low-speed UGV operating under different delay conditions, to identify a critical delay threshold that causes system instability.
- 2) We propose a genetic algorithm-based predictor framework to optimize the regularization parameters of a model-free predictor scheme, to improve prediction accuracy and eventually enhance the stability and transparency of teleoperated UGVs in the presence of delays.
- 3) We validate the GA-optimized predictor framework to compensate for the latency encountered during the operation of a low-speed teleoperated UGV on soft terrains for lunar exploration.

The article's structure is as follows. **Section II** delves into integrated system dynamics and controls for UGV bilateral teleoperation. **Section III** analyzes latency effects on bilateral teleoperation under varied conditions. **Section IV** conducts open-loop and closed-loop performance analyses of the GA-optimized predictor, demonstrating its compensatory efficiency. **Section V** presents experimental evaluation, comparing the predictor's performance with alternative strategies. Finally, **Section VI** summarizes findings and outlines future research directions.

## II. INTEGRATED SYSTEM DYNAMICS AND CONTROLS

The core of this research focuses on the end-to-end teleoperation of low-speed UGVs, incorporating force feedback for slippage awareness. The proposed system architecture, as illustrated in Fig. 1, comprises several key components that include the haptic device, the communication channel, low-speed UGV, soft terrain environment, and delay compensators.

### A. Haptic device Dynamics

In this study, the Phantom haptic device was utilized as the haptic interface. The Two-Degree Of Freedom (DOF) of the haptic device was employed to encode the linear and angular velocities of the UGV. This approach is commonly used in tele-driving UGV with non-holomorphic behavior [5]. The nonlinear dynamic equation of the Phantom haptic device was derived in detail in [6]

$$M_m \ddot{q}_m + C_m \dot{q}_m = u_m + f_h \quad (1)$$

$M_m$  represent the mass matrix of the robot,  $C_m$  denote the centrifugal matrix,  $q_m = [q_{m1} \ q_{m2}]^T$  is the joint position variable,  $u_m = [u_{m1} \ u_{m2}]^T$  is the joint control force, and  $f_h = [f_{h1} \ f_{h2}]^T$  represents the external force applied by human operator.

To address potential instability resulting from workspace mismatch between the master and the slave, a new dynamic variable was introduced,  $x_m = \lambda \dot{q}_m + q_m$  ( $0 < \lambda < 1$ ). As a result, the robot controller can be expressed as  $u_m = \bar{u}_m + u_m^*$ , where  $\bar{u}_m$  is the teleoperation controller, and  $u_m^*$  is the local controller, given by  $u_{mi}^* = B_{vi} \dot{q}_m + B_p q_m$ , as derived in [16]. Now, the velocity-velocity mapping coordination between the master and the slave becomes  $(x_{m1}, v_s)$  and  $(x_{m2}, \omega_s)$ .

The modified linear dynamics result in a first-order system as in (2).

$$\bar{M}_m \dot{x}_m + \bar{C}_m x_m = \bar{u}_m + f_h \quad (2)$$

where  $\bar{M}_m = M_m/\lambda$  and  $\bar{C}_m = C_m/\lambda$  are the equivalent mass and centrifugal, respectively.

### B. UGV Dynamics

For this research, the low-speed teleoperated UGV utilized was the Khalifa University (KU) rover model, which is an exact replica of the UAE Rashid rover [7]. The UGV's mobility concept relied on its kinematic models, especially at low speeds, which played a crucial role in ensuring stability and efficient locomotion. Inspired by the Boogie rover, the KU rover's locomotion principle assumes that the speeds of the front and rear wheels denoted as  $v_f$  and  $v_r$ , respectively, are nearly equal when operating on flat terrain. The kinematic model in (3), corresponding to pure rolling, is formulated in the UGV frame and provides an intuitive depiction of its movement characteristics [5].

$$\begin{bmatrix} v(t) \\ w(t) \end{bmatrix} = \begin{bmatrix} 1/2 & 1/2 \\ -1/2b & 1/2b \end{bmatrix} \begin{bmatrix} v_r(t) \\ v_l(t) \end{bmatrix} = \begin{bmatrix} v_d(t) \\ w_d(t) \end{bmatrix} \quad (3)$$

where  $v(t)$  and  $w(t)$  represent the measured longitudinal and angular velocity of the UGV, respectively.  $v_d(t)$ , and  $w_d(t)$  represent the desired longitudinal and angular velocity of the UGV, respectively.  $b$  is the distance between the right and the left wheels,  $v_r(t)$  and  $v_l(t)$  are the right and the left wheel velocities, respectively. The transformation matrix, denoted as  $E(b)$ , is:

$$E(b) = \begin{bmatrix} 1/2 & 1/2 \\ -1/2b & 1/2b \end{bmatrix} \quad (4)$$

On soft terrains, like deformable loose soil, the relationship between the linear velocity of each wheel and the product of the wheel's angular velocity and radius may not be equal due to wheel slippage caused by external forces from the soil. This deviation from the original kinematic model (in (3)) was recognized by Li et al. [15]. They proposed a modified kinematic model for the rover on soft terrains is expressed by (5).

$$\begin{bmatrix} v(t) \\ w(t) \end{bmatrix} = \begin{bmatrix} v_d(t) \\ w_d(t) \end{bmatrix} - E(b) \begin{bmatrix} v_{rd}(t) - v_r(t) \\ v_{ld}(t) - v_l(t) \end{bmatrix} \quad (5)$$

Now the slippage-induced loss of velocity on the UGV can be defined as:

$$\begin{bmatrix} \delta_v(t) \\ \delta_\omega(t) \end{bmatrix} = \begin{bmatrix} v_d(t) - v(t) \\ w_d(t) - w(t) \end{bmatrix} \quad (6)$$

The assumption is that the UGV has an in-built velocity controller, so the controlled input is  $u_s = [v_d \ \omega_d]^T$ . Additionally, in the study, the damping friction force exerted by the soft terrains on the wheel is considered as the environmental force (force feedback) for slippage awareness, represented as:

$$\begin{bmatrix} f_{ev}(t) \\ f_{e\omega}(t) \end{bmatrix} = \beta \begin{bmatrix} \delta_v(t) \\ \delta_\omega(t) \end{bmatrix} \quad (7)$$

where  $\beta$  is the damping coefficient of loose soil typically in the range of [0.5, 1.5].  $f_e = [f_{ev} \ f_{e\omega}]$  are the environmental force in the longitudinal and lateral direction, respectively.

### C. Bilateral Teleoperator Controls

The bilateral teleoperator system's controllers are synthesized based on the control theory approach, to ensure overall system stability. To achieve high performance and satisfactory transparency, the control system incorporates simple proportional controllers in both the haptic device (master) and the UGV (slave) to coordinate the pairs  $(x_{m1}, v)$  and  $(x_{m2}, \omega)$  in the presence of one-way communication delay  $T$  as outlined in (4) and (5), respectively.

#### • Master Controller

To achieve the perfect coordination between  $(x_{m1}, v)$  and  $(x_{m2}, \omega)$  at the operator side, the joint control input  $\bar{u}_m$  in (2) is computed based on the proportional control law as:

$$\begin{bmatrix} \bar{u}_{m1} \\ \bar{u}_{m2} \end{bmatrix} = \begin{bmatrix} -k_{m1} f_{ev}(t-T) \\ -k_{m2} f_{e\omega}(t-T) \end{bmatrix} \quad (8)$$

The proportional control gains  $k_{m1}$  and  $k_{m2}$  are designed to be positive definite.

#### • Slave Controller

To achieve the perfect coordination between  $(x_{m1}, v_d)$  and  $(x_{m2}, \omega_d)$  at the remote side. The input control  $\bar{u}_s$  in (8) is then computed based on the proportional control law as:

$$\begin{bmatrix} u_{s1} \\ u_{s2} \end{bmatrix} = \begin{bmatrix} k_{s1} x_{m1}(t-T) \\ k_{s2} x_{m2}(t-T) \end{bmatrix} \quad (9)$$

The proportional control gains  $k_{s1}$  and  $k_{s2}$  are designed to be positive definite.

In the designed aforementioned teleoperation system, when the desired linear velocity  $x_{m1}$  exceeds the actual linear velocity  $v$ , the human operator will feel a backward force pushing against the Joint 1 of the master robot. Similarly, when there is a difference between the desired angular velocity  $x_{m2}$  and the actual angular velocity  $\omega$ , a backward force will be felt on Joint 2. And vice-versa for the desired velocities is lower than the actual velocities [12], [15].

### D. Predictor Optimization

The basic structure of the model-free predictors utilized in this study was originally devised to tackle latency in high-speed teleoperated UGV systems in [9], [18]. The dynamics of the predictors are outlined in (10).

$$\begin{aligned} \dot{\hat{x}}_p(t) &= \dot{x}(t-T(t)) + \beta[x(t-T(t)) - x_p(t-T(t))] \\ \hat{x}(t) &= x_p(t) \end{aligned} \quad (10)$$

The predictor equation, (10), incorporates delayed signals  $x(t)$  and  $\dot{x}(t)$ , the previous value of the local state at a specific

time  $x_p(t - T(t))$ , the prediction for the current time  $x_p(t)$  and the regularization parameter  $\beta$ . The predictor demonstrates a good prediction performance within a bandwidth of 1Hz, which is acceptable for our coupling variables. However, in [16], the authors modified the dynamics by incorporating an additional degree of freedom to alleviate oscillatory error gain at higher frequencies, thus, improving prediction accuracy, adaptability, and handling larger delays. The modified predictor is represented by (11). Details of the predictor stability analysis can be found in [16].

$$\begin{aligned}\dot{x}_p(t) &= \dot{x}(t - T(t)) + \beta [x(t - T(t)) - x_p(t - T(t))] \\ &\quad + \alpha [\dot{x}(t - T(t)) - \dot{x}_p(t - T(t))] \\ \hat{x}(t) &= x_p(t)\end{aligned}\quad (11)$$

The delayed predicted signals from the previous instant are represented as  $\hat{x}_p(t - T(t))$  with a new regularization parameter  $\alpha$ . The authors further present a graph illustrating the relationship of these parameter values obtained through a linear relationship across various delay values [16]. However, these values are sub-optimal and slight deviation from the optimal values may significantly affect the prediction performance of the delay compensator. To address this issue, we propose a refined approach using GA, which is a promising meta-heuristic optimization technique employed to obtain optimal parameter values in parametric models [19].

In the context of fine-tuning parametric predictors, GA can be employed to search for the optimal values that minimize a specific objective function. By evaluating the fitness of candidate parameter sets, GA iteratively refines the parameter values to find the best configuration that optimizes the desired performance metric. In the parametric dynamics in (11), the two parameters  $\alpha$  and  $\beta$  are constrained to lie within specific value intervals:  $[\alpha_{\min}, \alpha_{\max}]$  and  $[\beta_{\min}, \beta_{\max}]$ , respectively. The extreme values within these intervals have been carefully selected to maintain marginal stability in the predictor system [16]. The overall cost function designed to compensate for the delays is given as:

$$f(\beta, \alpha) = w_1 \int_0^T t |x(t) - \hat{x}(t)| dt + w_2 \int_0^T \left| \frac{x(t) - \hat{x}(t)}{\hat{x}(t)} \right| dt \quad (12)$$

where the function  $f(\beta, \alpha)$  is the cost that needs to be minimized,  $t$  is the time variable,  $w_1$  and  $w_2$  are the weights assigned to each term to maintain a balanced trade-off between them. The former term measures the difference between the actual value  $x(t)$  at a specific time  $t$  and the predicted value  $\hat{x}(t)$  at the same time. And the latter term represents the overshoot reduction. Consequently, these cost function to be solved is directly converted into a fitness function to be minimized:

$$\text{Fit}(f(\beta, \alpha)) = f(\beta, \alpha) \quad (13)$$

To prioritize a better solution, the fitness function becomes:

$$\text{Fit}(f(\beta, \alpha)) = \begin{cases} f(\beta, \alpha) - v_{\min}, & f(\beta, \alpha) > v_{\min}, \\ 0, & \end{cases} \quad (14)$$

$v_{\min}$  in the above formula is the minimum estimates of  $f(\beta, \alpha)$ .

### III. EVALUATION OF DELAY IMPACT

In order to evaluate the impact of communication delays in the low-speed teleoperated UGV, the system paradigm of the integrated components (Red lines part) presented in Fig. 1 is simulated in Matlab/SIMULINK by using the above-discussed system dynamics and controls. The parameter values and coefficients of the system dynamics are taken from [20], while the control gains for the master and slave are set to  $k_m = 1$  and  $k_s = 4$ , respectively, to strike a balance between performance and transparency [12]. The evaluation metrics include velocity tracking ( $x_m = v_s$ ), transparency using force tracking ( $f_e = u_m$ ), and stability using the energy balance equation-based passivity theorem ( $E(t) = \int_0^t (x_m u_m - v_s f_e) dt$ ) [15]. The metrics are quantified using Mean Absolute Error (MAE), defined as follows:

$$MAE = \frac{1}{n} \sum_{t=1}^n |x_t - \hat{x}_t| \quad (15)$$

where  $n$  is the number of samples,  $x_t$  is the actual value, and  $\hat{x}_t$  is the delayed value.

#### A. No Delays

A sinusoidal operator force,  $F = 10\sin(\omega t)$ , is given as the input to the teleoperation system, and  $\omega$  is chosen to be 2 rad/s, which is similar to the real transmitted signals frequency of 0.5Hz. Assume no communication delays. The performance of velocity and force feedback tracking in the bilateral teleoperation system under this baseline condition is illustrated in Fig. 2. The output trajectories of Joint 1 and Joint 2 closely matched their respective reference trajectories in both the system performance. However, upon closer examination of the zoomed-in plots, a noticeable difference of 0.06 seconds can be observed between the output trajectories of velocity tracking, resulting in a small error evident in Table I. It is worth noting that this notable delay can be attributed to the inclusion of control gains designed to prioritize force feedback tracking over velocity tracking. Thus, achieving excellent performance and decent transparency.

Furthermore, in the shaded windows in Fig. 2, two distinct pulse disturbances were introduced to represent an environmental force. These disturbances occurred precisely at 4.0 and 7.0 seconds and were felt by the operator at the same time, as evident in the force tracking. As a result of these disturbances, the output velocity experienced a decrease at those specific time points, as indicated by the velocity tracking. This decrease in velocity causes the slippage. Moreover, the computed energy balance within the entire system, as shown in Fig. 4, proves that the closed-loop teleoperator is passive, and evidently guarantees the system stability.

#### B. Constant Delays

Three sets of simulation configurations were conducted, each with different constant time delays of 0.2, 0.6, and 1.0

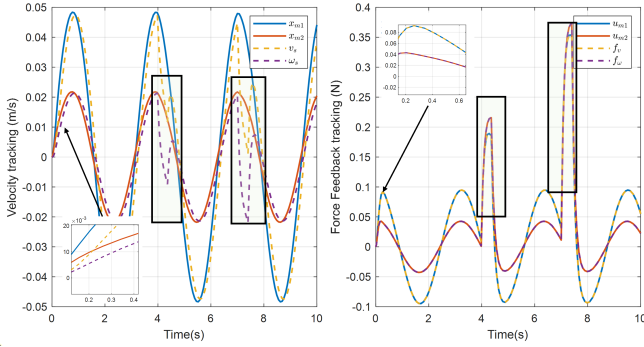


Figure 2: No delay case (solid lines - operator side and dashed lines - remote side): Velocity tracking performance (Left) and Force feedback tracking performance (Right) of both Joint 1 and Joint 2.

seconds. For each case, velocity tracking and force feedback tracking were evaluated. Specifically, Fig. 3 illustrates the delay cases of 0.6 seconds. From these simulation results, it is evident that this distinct delay was accurately identified and pin-pointed in addition to the nominal delay of 0.06 seconds in velocity tracking. Additionally, it was observed that as the delay increased, the deviation of the output trajectories from the reference trajectories also increased. To quantify these deviations, the MAE errors of these metrics are summarized in Table I. In the no-delay case, it is assumed that the results for all metrics are negligible for both joints, indicating perfect tracking performance. However, when a 0.2-second delay is introduced, significant deviations from the reference values of 0.0 can be observed. Specifically, for Joint 1 and 2, the MAEs of velocity tracking are  $18 \times 10^{-3} m/s$  and  $10 \times 10^{-3} m/s$ , respectively. Additionally, the MAEs of force feedback tracking are  $50 \times 10^{-3} N$  and  $41 \times 10^{-3} N$ , respectively. These values indicate a substantial deviation from the desired reference values. Moreover, in the case of a 1.0-second delay, the output distortion becomes even more significant. Furthermore, it is worth noting that the impact of the delay is more severe on the force feedback tracking compared to the velocity tracking. In the instant described above, the changes in the force feedback error values are almost ten times greater than those in the velocity tracking. Thus, we can say as the delay increases, the tracking error also increases. This resulted in a decrease in both performance and transparency.

To assess the stability of the delayed system, the energy balance analysis was conducted for all the experiments, as shown in Fig. 4. It was observed that as the delay increased, the energy balance within the system started to deviate from a positive balance (i.e. passive). At around a delay of 0.6 seconds, the system began losing its positive energy balance, indicating potential instability. The critical point was identified at approximately 0.72 seconds, where the energy balance reached zero and the system became non-passive. To further support this hypothesis, the phase margin of the closed-loop system with a 0.72-second delay was found to be approximately  $-0.115^\circ$ , as depicted in Fig. 5. Thus, all delays above this value make the system to exhibit a negative energy

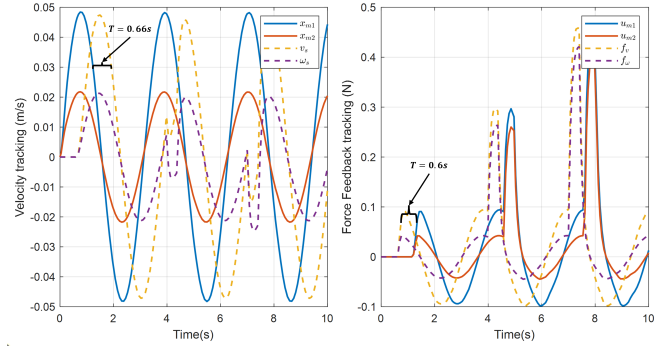


Figure 3: 0.6-second constant delay case: Velocity tracking performance (Left) and Force feedback tracking performance (Right) of both Joint 1 and Joint 2.

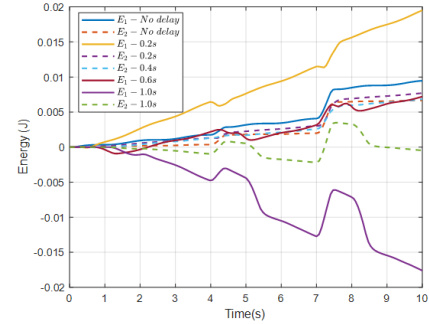


Figure 4: Energy balance Analysis for different constant delays: solid line - Joint 1 and dashed line - Joint 2

balance.

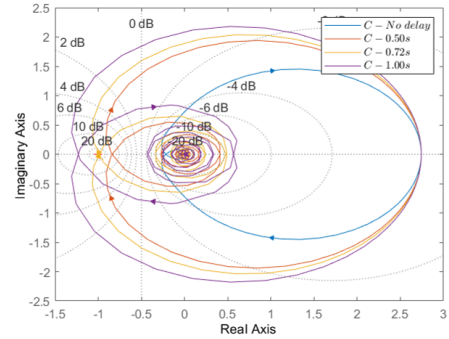


Figure 5: Nyquist plot for the closed-loop teleoperation system for different constant delays

### C. Varying Delays

Network delays are rarely constant and can fluctuate over time due to various factors. Thus, in this section, we conducted another three experiments with varying delays modeled as a uniform distribution between a minimum value  $a$  and a maximum value  $b$ :  $D \sim \mathcal{U}(a, b)$ . These delays included  $0.2 \sim \mathcal{U}(-0.1, 0.1)$ ,  $0.6 \sim \mathcal{U}(-0.1, 0.1)$ , and  $1.0 \sim \mathcal{U}(-0.1, 0.1)$  seconds. The same simulation condition and settings were maintained as in the constant delay case. For each case, the velocity tracking and force feedback tracking were evaluated, similar to the previous evaluations. The results of  $1.0 \sim \mathcal{U}(-0.1, 0.1)$  second is depicted in Fig. 6, which demonstrates

Table I: MAE Performance Metrics in Simulation

Cases	Delays (s)	Velocity tracking error ( $\times 10^{-3}$ m/s)		Force Feedback tracing Error ( $\times 10^{-3}$ N)	
		Joint 1	Joint 2	Joint 1	Joint 2
No delay	0.0	0.00003	0.00001	0.0	0.0
Constant delay	0.2	18.5	10.3	50.1	41.4
	0.6	38.1	19.0	122.7	92.4
	1.0	54.0	26.3	157.1	108.9
Varying delay	$0.2 \pm 0.1$	17.5	9.2	39.0	33.4
	$0.6 \pm 0.1$	36.2	17.6	109.6	76.4
	$1.0 \pm 0.1$	52.8	24.9	137.5	90.1
Compensated delay	0.6	17.3	8.7	25.4	19.8
	0.8	22.2	10.5	38.9	29.4
	1.0	27.8	14.1	51.5	32.1

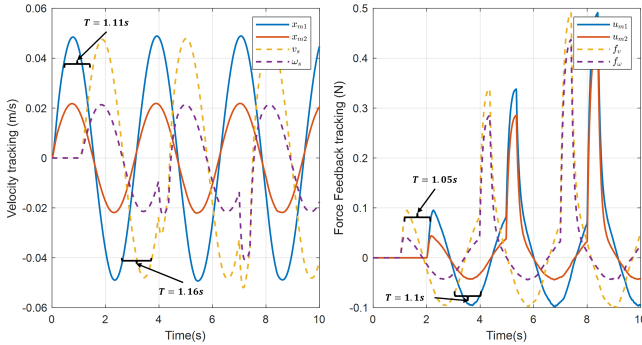


Figure 6: 1.0  $\sim \mathcal{U}(-0.1, 0.1)$ -second varying delay case: Velocity tracking performance (Left) and Force feedback tracking performance (Right) of both Joint 1 and Joint 2.

the impact of delay variations on the system performance. Notably, the varying delays at different time points were accurately identified and pin-pointed, and the nominal delay of 0.06 seconds in velocity tracking remained evident. Furthermore, as the delay increased, the deviations between the output trajectories and reference trajectories became more pronounced, the same as before. based on the summarized MAE error in Table I, it is observed that in the case of a  $0.2 \sim \mathcal{U}(-0.1, 0.1)$ -second delay, significant distortion from the reference values can be noted. Specifically, for Joint 1 and 2, the MAEs of velocity tracking are  $17.4 \times 10^{-3}$  m/s and  $9.2 \times 10^{-3}$  m/s, respectively. Additionally, the MAEs of force feedback tracking are  $39.0 \times 10^{-3}$  N and  $33.0 \times 10^{-3}$  N, respectively. These values indicate deviations from the reference values, although to a lesser extent compared to the constant delay case. Similar observations can be made for other cases as well. This finding supports the results obtained in [8]. Nevertheless, looking at the energy balance analysis presented in Fig. 7, the system exhibits similar characteristics to those observed in the case of constant delays. Thus, this finding indicates that variations in delays have a detrimental impact on the overall performance and stability of the teleoperation system.

#### IV. ANALYSIS OF DELAY PREDICTOR PERFORMANCE

In this section, we utilized the GA methodology described in the previous section to obtain the optimal predictor parameters,

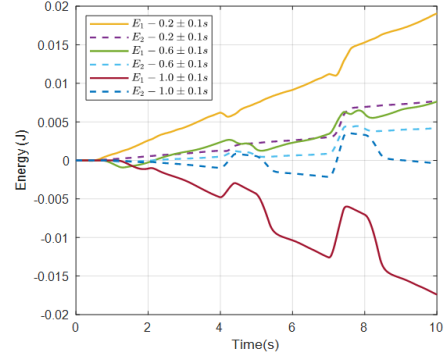


Figure 7: Energy balance Analysis for different Varying delays: solid line - Joint 1 and dashed line - Joint 2

$\alpha$  and  $\beta$ , for the delays that induce instability in the proposed low-speed teleoperated UGV. Specifically, the constant delays compensated were 0.6, 0.8, and 1.0 seconds. As suggested by the authors in [16], the fine-tuning process should begin with analyzing the open-loop step response of the predictor for the anticipated time delays. Subsequently, then completed using a simulation model of the closed-loop bilateral teleoperation system. Moreover, in addition to the metrics previously used, we will now introduce the Mean Absolute Percentage Error (MAPE) to evaluate the prediction accuracy and Mean Delay Compensation Percentage (MDCP) to quantify the reduction in delay achieved:

$$MAPE = \frac{1}{n} \sum_{t=1}^n \left| \frac{x_t - \hat{x}_t}{x_t} \right| \times 100\% \quad (16)$$

where  $n$  is the number of samples,  $x_t$  is the actual value, and  $\hat{x}_t$  is the predicted value.

$$MDCP = \left| \frac{T - T_c}{T} \right| \times 100\% \quad (17)$$

where  $T$  denotes the mean original delay and  $T_c$  denotes the mean compensated delay.

##### A. Open-Loop Performance Analysis

The proposed GA algorithm is then executed, resulting in the best designs for the open-loop step response of the predictor for the three delay cases, which are presented in Table II. These best parameter values obtained are compared with the parameter values acquired from the approximate linear relationships derived from the predictor [16]. Furthermore, the graphical open-loop performance of these optimal parameters is presented in Fig. 8. The simulation results clearly demonstrate that the GA-optimized predictor exhibits superior performance compared to the existing predictor across all delay cases. A closer examination of the zoomed-in plot reveals that the optimal predictor demonstrates a MAPE of 7.1%, whereas the existing predictor exhibits 14.6% in Fig. 8(a). These values correspond to the MDCP of 94% and 72%, respectively. A similar trend is observed for the cases of Fig. 8(b) and Fig. 8(c), 92% and 59%, and 89% and 53%, respectively. However, it is worth noting that as the delay increases, the difficulty of compensation becomes more

apparent, resulting in an overshoot, as seen in the case of a 1-second delay in Fig. 8 (c). For further clarity, the L2 norm of the tracking error is evaluated and presented in Fig. 9. It can be observed that as the delay increases, the error in compensating for the delay also increases. Surprisingly, the study reveals that the error difference remains consistent across various delay cases. For instance, in the 0.6-second delay, the optimal predictor has an L2-norm of 1.49, while the existing predictor has 6.02, a difference of 4.53. A similar pattern is observed in the 1.0-second delay scenario, with a difference of 4.68. These small variations indicate the impact of overshoot on delay compensation.

Table II: Optimal Parameters Vs Existing Parameters

Delays (s)	Optimal Parameters (GA)	Existing Parameters (Approx. Relationship) [16]
0.6	$\alpha = 0.62$ $\beta = 1.92$	$\alpha = 0.40$ $\beta = 2.87$
0.8	$\alpha = 0.49$ $\beta = 1.63$	$\alpha = 0.30$ $\beta = 2.09$
1.0	$\alpha = 0.57$ $\beta = 1.12$	$\alpha = 0.21$ $\beta = 1.94$

### B. Closed-Loop Performance Analysis

To evaluate the performance of the GA-optimized predictor and complete the tuning of its parameters for compensating the latency in our specific bilateral teleoperation system, we simulate the integrated components of the system paradigm shown in the Green lines section of Fig. 1. The parameter values and coefficients of the system dynamics and controls remain unchanged, as mentioned in the previous section. In our case study, the two predictors depicted in Fig. 1 are designed to predict different coupling variables. The forward predictor aims to estimate the linear velocity command  $x_{m1}$  and angular velocity  $x_{m2}$ , while the backward predictor estimates the longitudinal force feedback  $f_v$  and lateral force feedback  $f_\omega$ . From a preliminary test done, all these coupling variables have frequencies lower than 1Hz.

To ensure a fair comparison with the previous evaluations of the delayed system, we maintained the same simulation conditions and settings as described above. We then evaluated the velocity tracking and force feedback tracking for each case with the MAE metric. Initially, we used the optimal parameter values obtained from the open-loop analysis of the predictor. However, as the evaluation progressed, we made little adjustments to some of the predicted signals by modifying the predictor's parameter values, this is because of their slightest difference in their frequencies. The simulation results in Fig. 10, demonstrate the ability of the GA-optimized predictor to compensate for the 1.0 second delay. The predicted output trajectories of Joint 1 and Joint 2 closely matched their respective reference trajectories with an average MAPE of 8.3% and MDCP of 86 % in the case. In the force tracking, it is vividly shown that the predictor was able to predict the force feedback just before the actual force feedback at 6.0 seconds in Fig. 10. These observations indicate the effectiveness of the predictor, resulting in accurate tracking of the desired trajectories. In contrast, the delayed

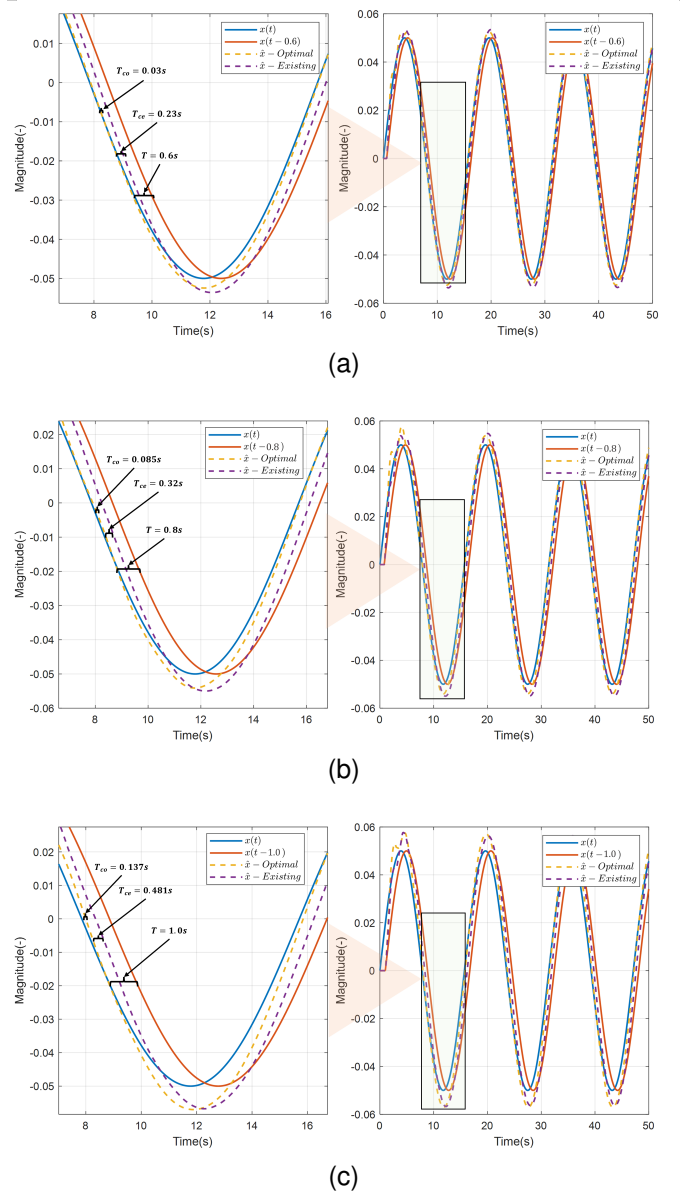


Figure 8: Open-loop prediction performance: Left- zoomed-in plot and Right- main plot (a) 0.6-second delay (b) 0.8-second delay (c) 1.0-second delay

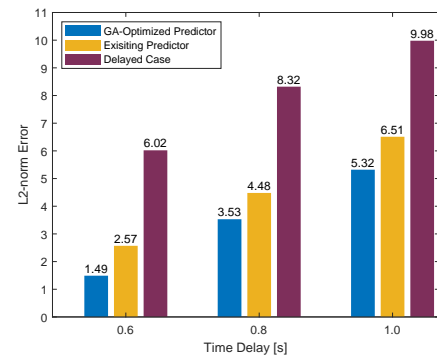


Figure 9: L2-norm Error under Three Time Delay conditions for Optimal Predictor, Existing Predictor, and No Predictor.

system achieved a MAPE of 28% in matching the reference trajectories. Furthermore, it was observed that a higher delay

resulted in the predictor exhibiting an increased overshoot. This highlights the trade-off between achieving accurate delay compensation and maintaining stability.

Upon analyzing the MAE errors in Table I for the 0.6-second delay case, the observed deviation from the reference values is almost negligible. Specifically, for Joint 1 and 2, the MAEs of velocity tracking are  $17.3 \times 10^{-3} \text{ m/s}$  and  $8.7 \times 10^{-3} \text{ m/s}$ , respectively. Additionally, the force feedback tracking error are  $25.4 \times 10^{-3} \text{ N}$  and  $19.8 \times 10^{-3} \text{ N}$ , respectively. The deviations are considered acceptable since they are significantly lower than those observed in the delayed case. Similar observations can be made for the 0.8-second and 1.0-second delay cases. Moreover, it has been demonstrated that the delays of 0.6, 0.8, and 1.0 seconds are no longer a threat to the stability of the compensated system. This is evident from the positive energy balance (passive) exhibited by the system, as shown in Fig. 11. However, it was observed that as the delay increases, the energy balance of the compensated system also increases. This phenomenon is attributed to the increased overshoot that accompanies increasing delays.

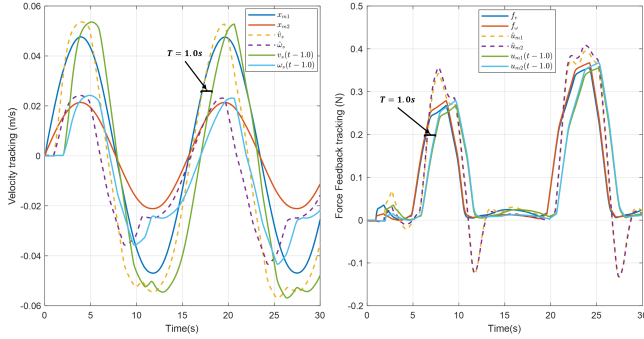


Figure 10: 1.0-second Compensated delay case: Left - Velocity tracking performance and Right - force feedback tracking performance of both Joint 1 and Joint 2

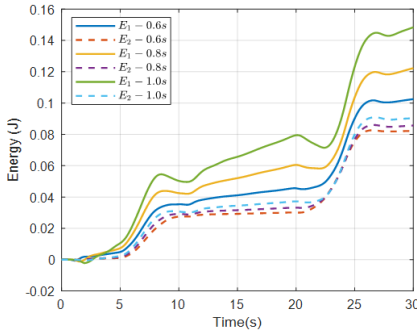


Figure 11: Energy balance Analysis for different delays with compensators: solid line - Joint 1 and dashed line - Joint 2

## V. HUMAN-IN-THE-LOOP EXPERIMENT

In this section, we conducted an experimental evaluation of the proposed GA-optimized predictor. The experimental setup consisted of the Torch-X haptic device, Matlab/SIMULINK software, and the Vortex Studio real-time simulator [12], [15], [21], which have demonstrated its high-fidelity and realistic simulation capabilities for UGVs operating on soft terrains.

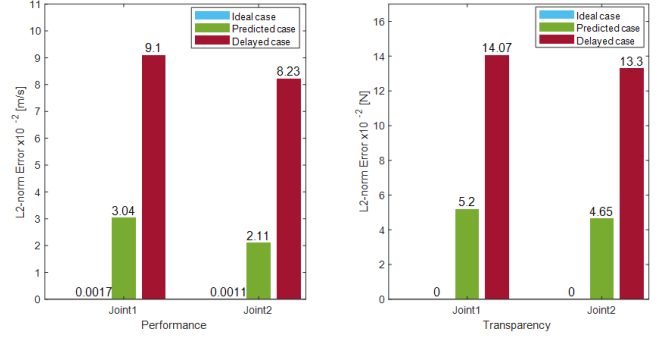


Figure 12: L2-norm error comparison for all the simulated cases across 1.0-second delay

We utilized the KU rover simulation environment specifically designed for analyzing mobility and traction on soft terrains in a real-time. This simulation method was previously developed and validated in an experimental study [22] conducted on a single-wheel testbed for the UAE Rashid Rover.

Fig. 13 presents a visual illustration of the experimental setup for the low-speed teleoperated UGV. The figure shows the various components and equipment used in the experimental setup. This setup enables control and interaction with the UGV in a simulated environment, providing a platform for evaluating the performance of developed algorithms for the teleoperated system. In our case study, we assume a low-speed teleoperated UGV for navigating the “Low-light” lunar environment known as Lacus Somniorum [7]. The one-way communication delay is anticipated to be around 0.98 secs representing a long-distance (380,000 Km) network. Thus, we used a varying transport delay of  $1.0 \sim \mathcal{U}(-0.1, 0.1)$ . The teleoperator controller gains in (8) and (9) were set to the different values used in the simulation,  $k_m = k_s = 4$ . This choice was made to achieve a balanced trade-off between performance and transparency. Measuring the force directly perceived by the operator is impractical. Instead, an estimation approach is employed, following the methodology described in [15], which relies on the underlying dynamics estimation.

$$f_h = \bar{M}_m \dot{x}_m + \bar{C}_m x_m - \bar{u}_m \quad (18)$$

Three distinct experimental configurations were conducted to comprehensively evaluate the system performance under diverse conditions. These configurations maintained consistent characteristics throughout the experiment that include trained-operator, and the soil properties characterized by looseness [22]. The Three configurations encompassed the following cases: (I) Instant case, (II) Delayed case, and (III) Predicted case. In addition to the previously used metrics above, two additional metrics, namely the success rate and task accomplishment time as mathematically described below, were employed to enhance the evaluation.

$$S_r = \left(1 - \frac{T_a - T_p}{T_p}\right) \times 100\% \quad (19)$$

where  $S_r$  is the mission success rate,  $T_a$  is the task accomplishment time with slippage and  $T_p$  is the ideal case,

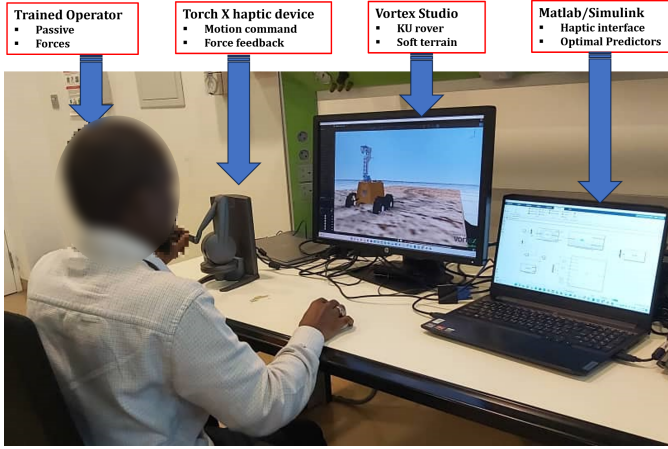


Figure 13: Experimental set-up with virtual low-speed teleoperated UGV

which is the task accomplishment time with pure rolling. An ideal experiment was conducted for the UGV traversing terrain from any point **A** to another point **B** in a straight line with pure rolling, and the task accomplishment time was recorded to be 200 seconds.

#### Case I: Instant Case

In this Ideal case, the UGV is being teleoperated to traverse the soft terrain with instant haptic feedback. The haptic feedback provides the operator with slippage awareness in both the longitudinal and lateral motion of the UGV. The deviation of the motion commands observed is well-regulated, as evident in Fig. 14(a). This is because the operator is able to well perceive the slippage as demonstrated by force tracking performance in Fig. 14(b), and use this awareness to correct the velocity commands and compensate for the deviation. Thus, the ideal bilateral teleoperator experimentally demonstrates excellent performance and satisfactory transparency, which is consistent with the simulation results shown in Fig. 2. This is quantitatively evident from the L2-norm error values of 0.378 m/s for linear speed and 7.87 rad/s for angular speed, as in Fig. 18-left. Additionally, 1.198 N for longitudinal force feedback, and 6.558 N for lateral force feedback, as illustrated in Fig. 18-right. Thus, these values indicate that the teleoperator's outputs closely align with the desired reference values.

The task completion time was recorded as 219 seconds, and the estimated mission success rate was 91.5%. These observations indicate a high likelihood of achieving the desired outcome. Furthermore, the energy balance of the bilateral teleoperator was computed. The results, as depicted in Fig. 17, reveal a positive energy balance, indicating that the system is passive and, therefore stable.

#### Case II: Delayed Case

As previously mentioned, the latency for this case study is assumed to be a uniform distribution of  $1.0 \sim \mathcal{U}(-0.1, 0.1)$  seconds. The obtained results for velocity tracking performance in Fig. 15(a) clearly demonstrate extremely poor performance, which confirms the simulated results shown in Fig 6.

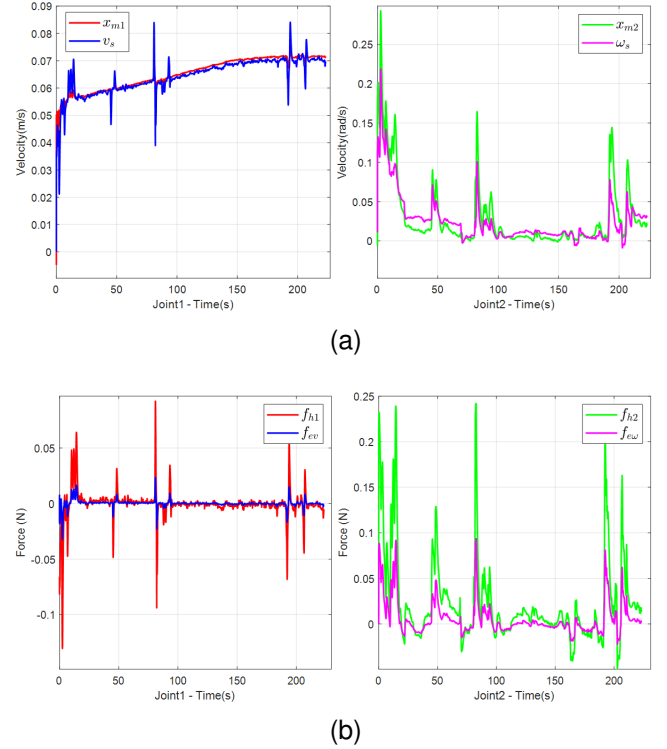


Figure 14: UGV traversing soft terrain with undelayed slippage awareness (a) Linear velocity tracking (Left) and Angular velocity tracking (Right) (b) Longitudinal force feedback tracking (Left) and Lateral force feedback tracking (Right)

The significant delays in the system witnessed in the zoomed-in plot confuse the operator, causing them to apply rapid and unpredictable changes in motion commands, which ultimately leads to over-speeding of the UGV at 0.2 m/s. Additionally, when examining the force tracking performance in Fig. 15(b), it is evident that the transparency of the system is almost null. The operator tries to perceive changes in the interaction forces, but due to the delayed force feedback received, they face difficulties in accurately compensating for the motion commands while trying to adapt to the delayed feedback. This leads to both over-compensation and under-compensation phenomena. The L2-norm error value of this performance and transparency are obtained from Fig. 18: 5.43 m/s for the linear velocity, 48.64 rad/s for the angular velocity, 24.64 N for the longitudinal force feedback, and 28.99 N for the lateral force feedback.

The task completion time and the mission success rate remained null in this case because the UGV became trapped in a sand trap before reaching the designated destination point. This unexpected event prevented the completion of the task and resulted in a mission failure. Additionally, the energy balance of the closed-loop system was computed to be negative, as depicted in Fig. 17. This indicates that the system is non-passive and, therefore unstable. Hence, we can attribute this primarily large delays between the operator and the UGV.

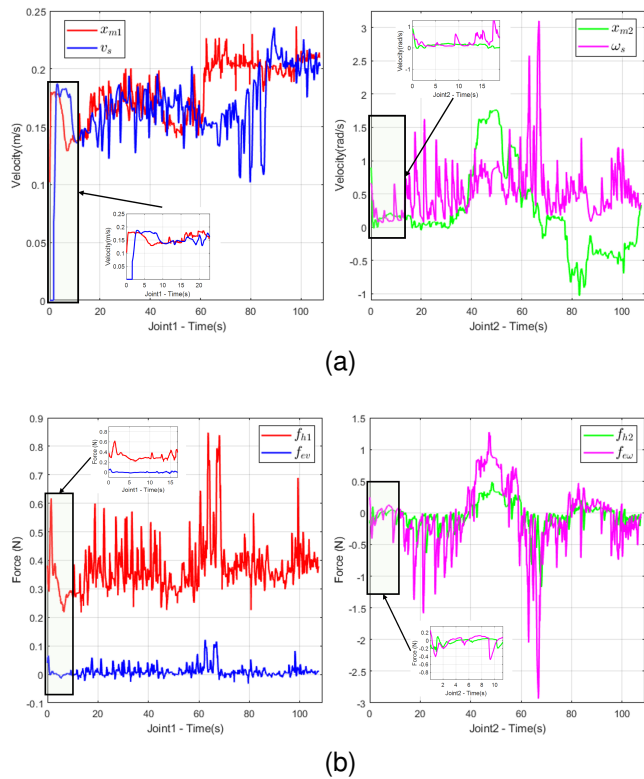


Figure 15: UGV traversing soft terrain with delayed slippage awareness. (a) Linear velocity tracking (Left) and Angular velocity tracking (Right) (b) Longitudinal force feedback tracking (Left) and Lateral force feedback tracking (Right)

### Case III: Predicted Case

This case highlights the main contribution of this work, which is the integration of the developed GA-optimized predictor framework into the closed-loop system to compensate for the delays encountered in Case II. The optimal parameter values of the predictors are  $\alpha = 0.57, \beta = 1.12$  for the forward predictor,  $\alpha = 0.64, \beta = 0.91$  for the backward predictor, as they exhibit different bandwidths as demonstrated in the closed-loop performance analysis Fig. 10. By providing predicted motion commands to the UGV and predicted force feedback to the operator, the predictor framework improves the performance and transparency of the compensated closed-loop system in the presence of large delays as illustrated in Fig. 16. Looking at this obtained result, we can see a significant improvement in terms of both velocity tracking performance and force tracking performance compared with those obtained in Case II. However, the predictor framework exhibits rapid transient behavior for about 5 seconds before eventually reaching a steady state, as shown in the shaded portion. Moreover, the L2-norm error values are computed to be 0.921 m/s for linear speed and 12.15 rad/s for angular speed, as in Fig. 18-left. Additionally, the L2-norm error amounts to 4.32 N for longitudinal force feedback, and 13.52 N for lateral force feedback, as illustrated in Fig. 18-right. Comparatively, these values are significantly lower than those observed in Case II, while slightly higher than the values obtained in Case I.

The task completion time was recorded as 236 seconds, and the estimated mission success rate was 83.7 %. These observations indicate a high chance of achieving the desired outcome. Additionally, a positive energy balance was obtained for the compensated bilateral teleoperator, ensuring the passive stability of the system, as illustrated in Fig. 17. However, the observed increase in energy balance that was observed during the simulation is also evident in the experiment.

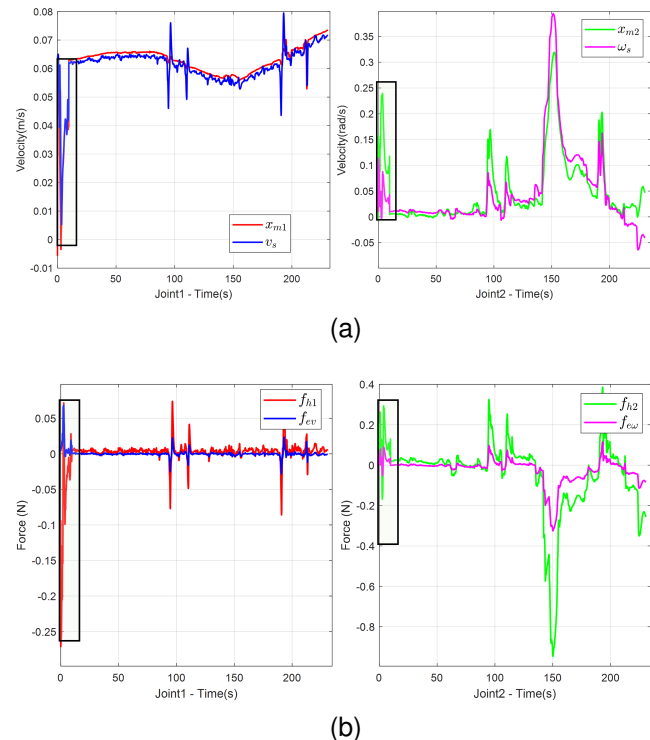


Figure 16: UGV traversing soft terrain with predicted slippage awareness. (a) Linear velocity tracking (Left) and Angular velocity tracking (Right) (b) Longitudinal force feedback tracking (Left) and Lateral force feedback tracking (Right)

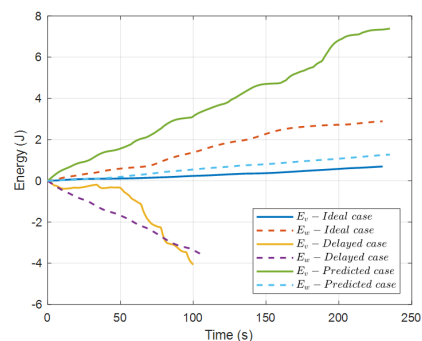


Figure 17: Comparison of Energy Balance among Ideal, Predicted, and Delayed Cases

## VI. CONCLUSION

The study focused on the impact of latency on bilateral teleoperation of low-speed UGVs on soft terrains. Our result reveals maintaining a latency threshold of 0.72 seconds is crucial for stable UGV operation. Furthermore, we proposed

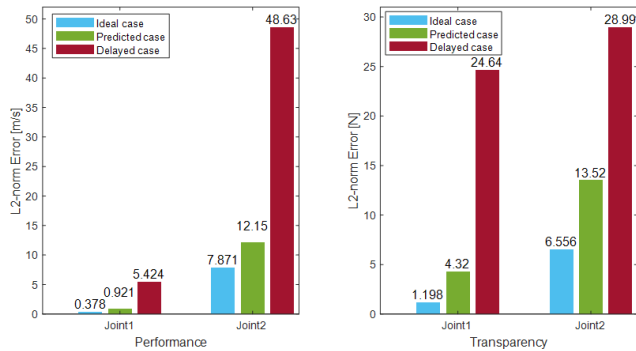


Figure 18: L2-norm error comparison for all the Experimented cases

a GA-optimized predictor framework to compensate for a 1.0-second latency in Lunar exploration, achieving a significant 86% latency compensation, outperforming the existing predictor's 51% in a closed-loop teleoperation system. Experimental validation of the framework demonstrated its effectiveness in compensating for delays in real-world scenarios. However, the proposed predictor has a notable limitation, characterized by increased overshoot and unused energy at higher delays. To address this in the future, a potential enhancement strategy could involve utilizing a Recurrent Neural Network (RNN) for modeling to capture the system complexity.

## REFERENCES

- [1] Li C, Tang Y, Zheng Y, Jayakumar P, Ersal T. "Modeling Human Steering Behavior in Teleoperation of Unmanned Ground Vehicles With Varying Speed". *Hum Factors*. May. 2022.
- [2] E. Ca, "Recent advances in research teleoperation, telepresence, and virtual reality" *Robotic Teleoperation and Telepresence, Carlos III University, Madrid*, December 2016.
- [3] S. N. F. Nahri, S. Du, and B. J. Van Wyk, "A Review on Haptic Bilateral Teleoperation Systems," *J. Intell. Robot. Syst. Theory Appl.*, vol. 104, no. 1, 2022.
- [4] S. Opiyo, J. Zhou, E. Mwangi, W. Kai, and I. Sunusi, "A Review on Teleoperation of Mobile Ground Robots: Architecture and Situation Awareness," *Int. J. Control. Autom. Syst.*, vol. 19, no. 3, pp. 1384–1407, 2021.
- [5] W. Li, N. Yang, J. Wang, and D. Ren, "Kinematic Teleoperation of Wheeled Mobile Robot with Slippage Compensation on Soft Terrains," *IEEE Access.*, vol. 7, pp. 110982–110991, 2019.
- [6] W. Li et al., "Semi-autonomous bilateral teleoperation of six-wheeled mobile robot on soft terrains," *Mech. Syst. Signal Process.*, vol. 133, p. 106234, 2019.
- [7] R. Almehsini, P. Garg, and M. Wali, "Thermal Management System Design and Analysis of Rashid Rover - Emirates Lunar Mission," *Proc. Int. Astronaut. Congr. IAC*, vol. C2, no. October, 2021.
- [8] Y. Zheng, M. J. Brudnak, P. Jayakumar, J. L. Stein and T. Ersal, "A Predictor-Based Framework for Delay Compensation in Networked Closed-Loop Systems," in *IEEE/ASME Transactions on Mechatronics*, vol. 23, no. 5, pp. 2482-2493, Oct. 2018.
- [9] Y. Zheng, M. J. Brudnak, P. Jayakumar, J. L. Stein and T. Ersal, "A Delay Compensation Framework for Predicting Heading in Teleoperated Ground Vehicles," in *IEEE/ASME Transactions on Mechatronics*, vol. 24, no. 5, pp. 2365-2376, Oct. 2019.
- [10] G. Graf, H. Xu, D. Schitz and X. Xu, "Improving the Prediction Accuracy of Predictive Displays for Teleoperated Autonomous Vehicles," *2020 6th International Conference on Control, Automation and Robotics (ICCAR)*, Singapore, pp. 440-445.2020.
- [11] R. Luz, J. Corujeira, J. L. Silva and R. Ventura, "Traction Awareness Through Haptic Feedback for the Teleoperation of UGVs," *27th IEEE International Symposium on Robot and Human Interactive Communication (RO-MAN)*, Nanjing, China, pp. 313-31, 2018.
- [12] W. Li, L. Ding, Z. Liu, W. Wang, H. Gao, and M. Tavakoli, "Kinematic Bilateral Teledriving of Wheeled Mobile Robots Coupled with Slippage," *IEEE Trans. Ind. Electron.*, vol. 64, no. 3, pp. 2147–2157, 2017.
- [13] M. Sierotowicz, B. Weber, R. Belder, K. Bussmann, H. Singh, and M. Panzirsch, "Investigating the influence of haptic feedback in rover navigation with communication delay", vol. 12272 *LNCS. Springer International Publishing*, 2020.
- [14] Y. -J. Pan, C. Canudas-de-Wit and O. Sename, "A New Predictive Approach for Bilateral Teleoperation With Applications to Drive-by-Wire Systems," in *IEEE Transactions on Robotics*, vol. 22, no. 6, pp. 1146-1162, Dec. 2006.
- [15] W. Li, N. Yang, J. Wang, and Z. Deng, "Teleoperation of wheeled mobile robots subject to longitudinal slipping and lateral sliding by time-domain passivity controller." *Mechatronics.*, 81, 2022.
- [16] S. Guo, Y. Liu, Y. Zheng and T. Ersal, "A Delay Compensation Framework for Connected Testbeds," in *IEEE Transactions on Systems, Man, and Cybernetics: Systems*, vol. 52, no. 7, pp. 4163-4176, July 2022.
- [17] D. J. Gorsich, P. Jayakumar, M. P. Cole, C. M. Crean, A. Jain, and T. Ersal, "Evaluating mobility vs. latency in unmanned ground vehicles," *J. Terramechanics*, vol. 80, pp. 11–19, 2018
- [18] Y. Sato, S. Kashihara and T. Ogishi, "Implementation and Evaluation of Latency Visualization Method for Teleoperated Vehicle," 2021 IEEE Intelligent Vehicles Symposium (IV), Nagoya, Japan, pp.1-7, 2021.
- [19] M. Wakhaure, B. K. Patle, and A. K. Mahindrakar, "Application of AI techniques and robotics in agriculture: A review," *Artif. Intell. Life Sci.*, vol. 3, no. January, p. 100057, 2023.
- [20] M. C. Çavuşoğlu, D. Feygin and F. Tendick, "A critical study of the mechanical and electrical properties of the phantom haptic interface and improvements for high-performance control," *Presence: Teleoperators & Virtual Environments*, vol. 11, no. 6, pp. 555–568, 2002.
- [21] A. Peiret, E. Karpman, L. L. Kovács, J. Kövecses, D. Holz, and M. Teichmann, "Modelling of off-road wheeled vehicles for real-time dynamic simulation," *J. Terramechanics*, vol. 97, pp. 45–58, 2021.
- [22] A. Abubakar, R. Alhammadi H. Zweiri and L. D. Seneviratne, "Advance Simulation Method for Wheel-Terrain Interactions of Space Rovers: A Case Study on the UAE Rashid Rover ," *arXiv:2308.12431 [cs]*, Aug. 2023.



**Ahmad Abubakar, (Member, IEEE)** a Ph.D candidate at Khalifa University (KU), UAE, focuses on robotics, with specific emphasis on UGV, teleoperation, and control of time-delay systems. Holding a B.Eng. in Electrical Engineering from Bayero University Kano in 2014 and an M.Sc. in System, Control, and IT from the University Grenoble Alpes (UGA) in 2018, his journey is marked by a passion for mastering complex systems. Ahmad's pursuits extend to practical applications through an internship at GIPSA-Lab in France.



emphasis on applied AI

**Yahya Zweiri, Ph.D. (Member, IEEE)** obtained his Ph.D. degree in Mechanical Engineering from King's College London, in 2003. He is currently a Professor at the Department of Aerospace Engineering and the Director of the Advanced Research and Innovation Center, Khalifa University, United Arab Emirates. Dr. Zweiri is currently a professor with over 130 refereed journals and conference papers, as well as ten filed patents in the USA and UK. His primary research focus centers around robotic systems for challenging environments, with a specific emphasis on applied AI and neuromorphic vision systems.



**Ruqayya Alhammadi** is currently a PhD candidate at the Khalifa University (KU), Abu Dhabi, United Arab Emirates (UAE), specializing in the application of robotics in space-related projects, with specific emphasis particularly wheel soil interaction in space rovers. Her primary research focus centers on neuromorphic vision systems. Holding a B.Eng. in Mechanical Engineering with a minor in UAVs from Khalifa University in 2018 and an M.Sc. in Mechanical Engineering with concentration in spacecraft systems from Khalifa University in 2020.



**Mohammed B. Mohiuddin** is a PhD candidate at the Khalifa University (KU), UAE, specializing in the application of reinforcement learning to robotics. He earned his Bachelor of Engineering (B.E.) in Mechanical Engineering from Osmania University, India in 2017, securing the university's top rank, and his Master of Science (M.Sc.) in Aerospace Engineering from King Fahd University of Petroleum and Minerals (KFUPM), Saudi Arabia in 2020. His current research focuses on enhancing UAV autonomy and intelligence.



**Lakmal Seneviratne** is currently a Professor of mechanical engineering and the Founding Director of the Centre for Autonomous Robotic Systems (KUCARS), Khalifa University, UAE. He is also an Emeritus Professor at King's College London, U.K. He has worked as an Associate Provost for Research and Graduate Studies and an Associate VP Research at Khalifa University. Prior to joining Khalifa University, he was a Professor of mechatronics, and the Founding Director of the Centre of Robotics Research, King's College London. His main research

interests include robotics and automation, with particular emphasis on robotic systems interacting with complex dynamic environments. He has published over 400 peer-reviewed publications.